Heliyon 6 (2020) e05510

Contents lists available at ScienceDirect

Heliyon

journal homepage: www.cell.com/heliyon

Research article

Spectroscopic characterization of composite lithium materials irradiated with high-temperature plasma

V.P. Budaev [a,b,*], S.D. Fedorovich [a], A.V. Lubenchenko [a], A.V. Karpov [a,b], N.E. Belova [b], M.K. Gubkin [a]

[a] National Research University "MPEI", Moscow, Russia
[b] National Research Center "Kurchatov Institute", Moscow, Russia

ARTICLE INFO

Keywords:
Materials science
Plasma physics
X-ray photoemission spectroscopy
Lithium
Lithium carbonate
Plasma test
Plasma induced structure

ABSTRACT

High-temperature plasma irradiation of materials leads to significant modification of surface structure, growth of deposited composite films and surface layers with induced self-similar granularity on the scale from macroscales to nanoscale due to strong plasma-surface interaction. The aim of this study was to characterize lithium materials irradiated with high-temperature plasma in the T-10 tokamak and PLM device. The reactivity of lithium leads to reactions with impurities in the plasma and on the vessel. Post-mortem analyses by the X-ray photoemission spectroscopy and X-ray analysis have been used to identify deposits composition and morphology. Lithium carbonate composites have been detected by analysis demonstrating materials mixing and evidence of plasma-induced structure. New structures with the high specific surface area of hierarchical granular are registered. The reference industrial powder of lithium carbonate irradiated with steady-state plasma in the PLM device has acquired a new similar structure demonstrating universal influence of plasma on the structure of irradiated materials.

1. Introduction

High-temperature plasma irradiation of materials leads to a significant modification of surface structure [1, 2, 3, 4], growth of deposited composite films and surface layers with self-similar granularity [5, 6] on the scale from macroscales to nanoscale. The heterogeneous granularity of deposits was detected in tokamaks and fusion devices [4, 5, 6]. Such deposits of porous surfaces with a high specific area are a source of enhanced fuel gas retention which is the problem for a future fusion reactor since fuel gas (tritium) inventory has to be limited.

Plasma-surface interaction is sensitive to the surface roughness, it affects the parameters of the edge plasma and plasma confinement in the tokamak. The universal mechanism of surface growth (see, e.g. [1, 2, 7]) is considered to control a long-term evolution of the plasma-facing surface under the high-temperature plasma irradiation.

Plasma-facing materials should be examined with steady-state plasma to predict their behavior in plasma devices including the future fusion tokamak reactor.

Liquid lithium contained in capillary porous system [8, 9, 10, 11] is attractive as the first wall components for a future fusion reactor, which has been demonstrated in modern fusion devices - tokamaks T-10 [12, 13], T-11M [10, 14], FTU [15, 16], NSTX-U [17] and stellarator TJ-II [18, 19]. At the same time, due to quick reactions of lithium with impurities (oxygen, nitrogen, carbon etc.) the growth of solid deposits on the in-vessel components can reduce the advantageous effects of the lithium plasma-facing component operation. Lithium materials should be tested in modern tokamaks and plasma devices with steady-state plasma to simulate conditions in future fusion reactors. Detailed analysis of the chemical elemental composition of lithium materials irradiated with plasma could help to reveal a plasma-induced effect on the structure of deposits and their sustainability in future fusion devices. The results of such a study are presented in this article.

2. Experimental samples

The experimental conditions and samples from the T-10 tokamak and PLM plasma device are described in [20, 21]. The deposited specimens as thick layers of ~0.5–2 mm thickness of irregular shape are collected on in-vessel components of the T-10 tokamak. The analyzed lithium specimens were formed for a long time during the T-10 tokamak experimental

* Corresponding author.
E-mail address: budaev@mail.ru (V.P. Budaev).

https://doi.org/10.1016/j.heliyon.2020.e05510
Received 19 August 2020; Received in revised form 28 October 2020; Accepted 10 November 2020

campaign in 2016–2018 described in [12]. The purity of bulk deuterium plasma in T-10 tokamak during experiments was enough high: effective ion charge (Z_{eff}) was from 1,5 to ~4 in experiments. In these experiments, pure liquid lithium contained in capillary porous system used as the plasma facing material; liquid lithium evaporated under a powerful plasma load of repetitive plasma discharges of ~1 s duration and redeposited on the surface resulting in a growth of deposited solid composite films and surface layers. The reactivity of lithium has led to reactions with impurities in the plasma and on the vessel resulting in mixing of materials and plasma-induced structure of self-similar granularity on a scale from macroscale to nanoscale due to the strong plasma-surface interaction. The main source of carbon reacted with lithium inside T-10 vessel was the hydrocarbon films formed on in-vessel components and observed earlier, see [2, 3, 5]. Such carbon materials eroded under plasma load and re-deposited on the vessel reacting with lithium. This process of materials' deposition from plasma is considered to produce the composite materials [1, 2, 3]. The additional source of carbon might be as well the atmospheric gases after opening the tokamak vessel as was observed in HT-7 tokamak, see [22]. The source of carbon might be as well stainless steel as discussed in [23].

Porous and roughen irregular surface of lithium deposits were detected by the post-mortem scanning electron microscopy (SEM) (see details in [20, 21]) supposing the interaction of lithium with carbon and oxygen impurities in the plasma and on the vessel surface.

Lithium specimens from the T-10 tokamak were subsequently irradiated with plasma in PLM linear plasma device [24, 25]. The samples were irradiated with helium plasma of discharge duration up to 200 min with plasma parameters identical to edge plasma in a tokamak (see details of these experiments in [20, 21]).

The materials irradiated by T10 hold before irradiation in PLM plasma device in atmospheric gases during several days. As the material is highly porous after irradiation in T10, the atmospheric gases have diffused to the lithium specimens which can lead to additional chemical reactions. Such condition of in-vessel material's contact with atmospheric gases is typical during periodical conditioning of plasma devices, it is expected as well during future reactor operation.

Under the steady-state plasma load in PLM device, lithium, carbon, oxygen from exposed samples enter the plasma volume as was detected by plasma diagnostics [20]. Subsequent reactions of these chemical elements into the plasma volume and their deposition on the surface lead to new surface structures. Post-mortem analysis of the samples after plasma irradiation in PLM revealed a structural change in comparison with the original. Examples of SEM micrographs are in Figures 1 and 2. The SEM analysis of the sample surface has shown a reformation of the irregularity, cf. Figures 1 and 2. The structures demonstrate a hierarchical granularity over scales of ~0.5–500 microns [20, 21]. This granularity is similar to the structure of hydrocarbon deposits such as cauliflower-like previously observed in tokamaks and plasma devices [3, 5] under specific high-temperature plasma [26] impact. For comparative analysis, a reference industrial powder of lithium carbonate was irradiated with plasma in PLM device under the same conditions as examined samples from the T-10 tokamak. The structure of this reference powder also changed after this treatment, the surface structure after processing has acquired a similar structure, Figure 3.

3. XPS analysis

XPS spectra were recorded by means of the Nanofab 25 (NT-MDT) electron-ion spectroscopy platform (techniques are described in [27, 28, 29]). The experiments were performed in an ultra-high vacuum (10^{-7} Pa). X-ray source: SPECS XR 50, dual Al/Mg anode, non-monochromatic X-radiation, photon energies 1486.6 and 1253.6 eV; angle 54.7° relative to the analyzer axis. Energy analyzer: electrostatic hemispherical SPECS Phoibos 225; energy resolution 0.78 eV (about Ag $3d_{5/2}$); Fixed Analyzer Transmission (FAT) mode. Calibration positions: Cu $2p_{3/2}$ (binding energy 932.62 eV), Ag $3d_{5/2}$ (368.21 eV), and Au $4f_{7/2}$ (83.95 eV).

The specimens were sputtered by an ion source SPECSIQE 12/38: differential pumping; 99.9995% pure Ar; scanning area 2.8 mm × 4.0 mm; incidence angle 60° to the surface normal; ion energy 500 eV.

A comparative analysis of the chemical structure of the material has been fulfilled for the samples:

(i) lithium specimens from the T-10 tokamak, specimens were heated by plasma up to the temperature below ~200 °C,
(ii) lithium specimens from the T-10 tokamak subsequently irradiated with steady-state plasma in PLM device, exposed specimens were heated by plasma up to the temperature of ~700 °C,
(iii) reference high-purity industrial powder Li_2CO_3 (99.95%).

To compare the chemical structure of the surface matter and the bulk matter of the initial specimens from the T-10 tokamak, XPS analysis of (1) original (initial) specimens, (2) milled specimen, (3) specimen sputtered by argon (Ar) beam has been done.

The milled specimen was prepared by mechanical milling of the initial specimen. The sputtered specimen was prepared by sputtering the

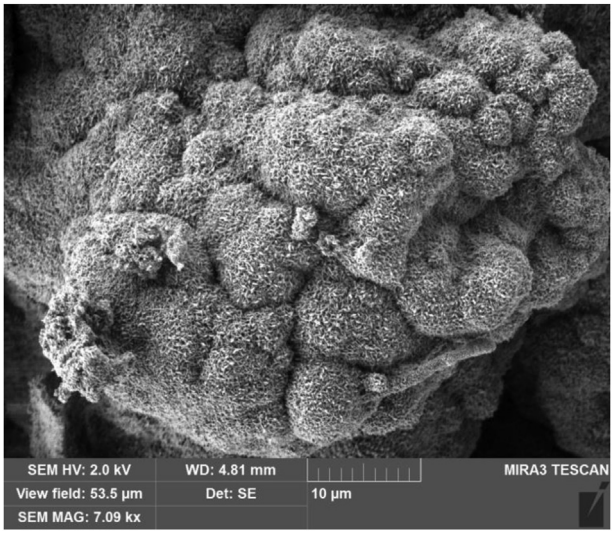

Figure 1. SEM micrograph of specimen deposited on plasma-facing vessel component in the T-10 tokamak experiments with the liquid lithium capillary-porous system operation.

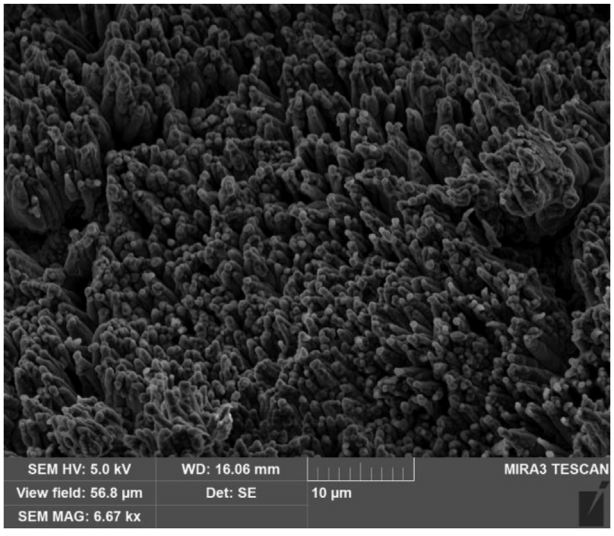

Figure 2. SEM micrograph of lithium specimen from the T-10 irradiated with helium plasma in the PLM plasma device for ~200 min.

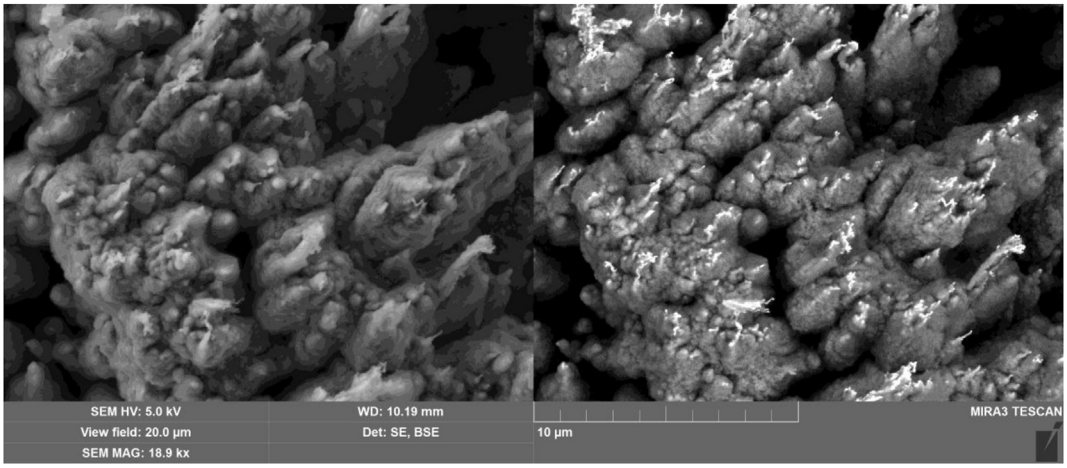

Figure 3. SEM micrograph of reference industrial lithium carbonate specimen irradiated with helium plasma in the PLM plasma device for ~200 min. Left- secondary electron (SE) analysis showing the topography; right - backscattered electron (BSE) analysis showing the composition to detect contrast between areas with different chemical compositions.

initial specimen with an Ar+ beam, the beam current was of ~1 μA, the sputtering time was 20 min.

Standard XPS analysis of all specimens has identified chemical elements like C, O, Li. Figure 4 shows spectra of lines C 1s, O 1s, Li 1s for the lithium specimens. The XPS data were used to estimate relative atomic concentrations in specimens (Table 1) demonstrating a deviation from the reference high-purity powder Li_2CO_3 due to a complex structure of Li_yCO_x. Such complex structure Li_yCO_x was investigated analyzing the XPS spectra.

XPS spectra were used for the characterization of the composition and bonding states of elements.

A photoelectron line of a specific element is decomposed into peaks related to chemical bonds (partial peaks). The peak shapes depend on chemical shifts, satellite peaks overlapping, sample charging, etc.

The method described in [27] was used for the deconvolution of XPS peaks.

As far as the specimens were dielectric, they were electrically charged by X-rays during the XPS analysis. The method for the correction of peak Li-O- of line O 1s was used to compensate for the influence of specimen charging. The value of binding energy of Li-O- line O 1s was taken from paper [30]. The result is shown in Figure 3. Other peaks of lines C 1s and Li 1s correspond to values of binding energies reported in [30] after that correction. For the sputtered sample, the Li_2O peak of the binding energy of 528.5 eV appeared on line O 1s that corresponded to data from paper [30].

The XPS method is not able to detect hydrogen isotopes in specimens. At the same time, the peak position is sensitive to chemical bonds of hydrogen isotopes with other elements. The data from paper [31] were used to detect bonds of hydrogen (like CH_x, $C(OH)_x$) in the XPS spectra. The values of the binding energy of lithium compounds and hydrocarbons are given in Table 2.

The XPS spectra of the initial specimen from the T-10 tokamak and the specimen irradiated with PLM plasma are shown in Figure 5. The spectra were analyzed by using the method developed in [27] to resolve the peaks and detect specific lines in the spectra. Line C 1s was deconvolved into partial peaks for all specimens using the method described in [27].

Partial relative concentrations *cp* of compounds were evaluated by using the decomposition results for all samples (Table 2). The calculated ratio of hydrocarbons (CH_x, $C(OH)_x$) concentration to that of carbonates is given in Table 2. This ratio for the reference sample differs significantly from other samples.

The reason is that the stoichiometric formula for lithium carbonate Li_yCO_x from T-10 is quite different from Li_2CO_3. We have to remind that the probing penetration depth of X-rays during the XPS analysis is of only a few nanometers. So, detected hydrocarbons are located only in a thin layer on the surface of specimens.

4. X-RAY analysis

The structures of experimental specimens in comparison with reference ones were studied by X-ray analysis, see Table 2:

(i) flake lithium specimens from the T10 tokamak (T10),
(ii) lithium specimens of large flakes (T10-PLM) from the T10 tokamak subsequently irradiated with plasma in PLM device
(iii) reference specimen (Li_{2CO3}) of high-pure industrial lithium carbonate as a powder,
(iv) reference specimen (Li_{2CO3}-PLM) of pure industrial Li_2CO_3 irradiated in the PLM device.

The specimens from the T10 tokamak (T10, T10-PLM) and reference industrial Li_2CO_3 specimen irradiated with plasma in the PLM device (Li_{2CO3}-PLM) were analyzed using the Rigaku Smartlab X-ray diffractometer with a rotating anode and using characteristic copper radiation CuKα1 (wavelength $\lambda = 1.54056$ Å, radiation energy 8.048 keV). The X-ray optics consists of the Goebel focusing parabolic mirror in the Bartels scheme, the double Ge 220 monochromator, a system of collimating slits and a scintillation detector. The sample was mounted in a 3-axis goniometer installed horizontally.

The Bruker-D8 diffractometer with a copper anode (wavelength $\lambda =$ 1.54056 Å) with horizontal arrangement of the specimen was used to analyze the reference sample of industrial powder Li_2CO_3 (Li_{2CO3}).

Industrial Li_{2CO3} specimen structure has base-centered monoclinic lattice and monoclinic space group C2/c. Normalized diffraction patterns of specimens are shown in Figure 6. All specimens studied have a monoclinic crystal lattice which is the feature of lithium carbonate Li_2CO_3. The diffraction patterns of specimens (T10), (T10PLM), and (Li_{2CO3} PLM) are characterized by unit cell dimensions $a = 8.39$ Å, $b =$ 5.00 Å and $c = 6.21$ Å, related with Li_2CO_3 structure [32]. The irradiated specimens' structure deviates from the structure of reference industrial Li_2CO_3 powder which has a monoclinic translation lattice reflections with unit cell dimensions $a = 8.29263$ Å, $b = 4.94743$ Å, $c = 6.1$ Å.

X-ray analysis of specimens (T10), (T10 - PLM), (Li_{2CO3}-PLM), Figure 6, did not reveal any hydrogen molecules included in the crystal structure.

Taking the specific area of powder is larger than that of the flakes, it helps to evaluate the distribution of elemental composition in depth.

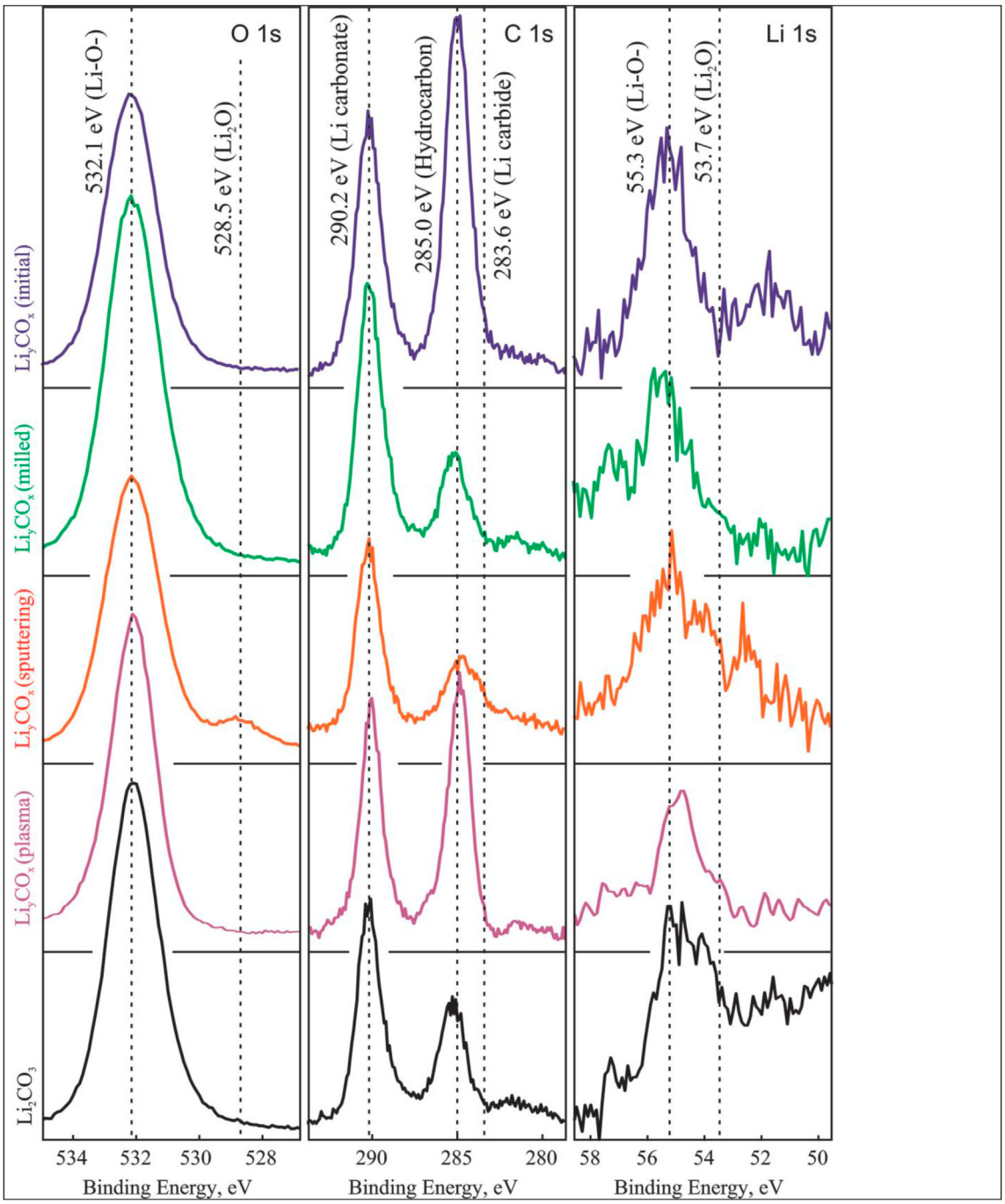

Figure 4. X-ray photoelectron spectra of O 1s, C 1s and Li 1s of samples: the initial specimen from the T-10 tokamak (initial), the milled specimen (milled), the specimen after sputtering (sputtering), the specimen irradiated with helium plasma in the PLM (plasma), the high-purity industrial lithium carbonate (Li_2CO_3).

Table 1. Relative atomic concentration c in specimens.

Chemical element	*c*, %				
	Li_yCO_x specimens from the T-10 tokamak				Reference industrial high-purity powder Li_2CO_3
	Initial (T10)	Milled	sputtered with Ar beam	irradiated with PLM plasma (T10-PLM), sample biasing voltage -20 V	
C	33.1	21.1	25.2	27.4	23.0
O	34.9	37.7	40.7	32.8	41.0
Li	32.0	41.2	34.1	39.8	36.0

Table 2. *Partial relative concentration c_p in specimens.*

Formula	Binding energy, eV	c_p, %				
		Li_yCO_x (specimens from the T-10 tokamak)				Reference industrial high-purity powder Li_2CO_3
		Initial (T10)	milled	sputtered with Ar^+ beam	Irradiated with PLM plasma (T10 PLM), sample biasing voltage -20 V	
LiC_x	283.6	-	-	7.9	-	-
CH_x	284.4	14.8	9.8	15.7	33.4	10.3
$C(OH)_x$	285.0	44.6	18.4	9.3	18.6	25.3
-C=O	287.9	-	4.0	0.6	1.5	3.3
Li_yCO_x	290.1	40.6	67.8	66.5	46.5	61.1
		Ratio of hydrocarbon concentration to carbonate concentration				
		1.46	0.42	0.38	1.11	0.58

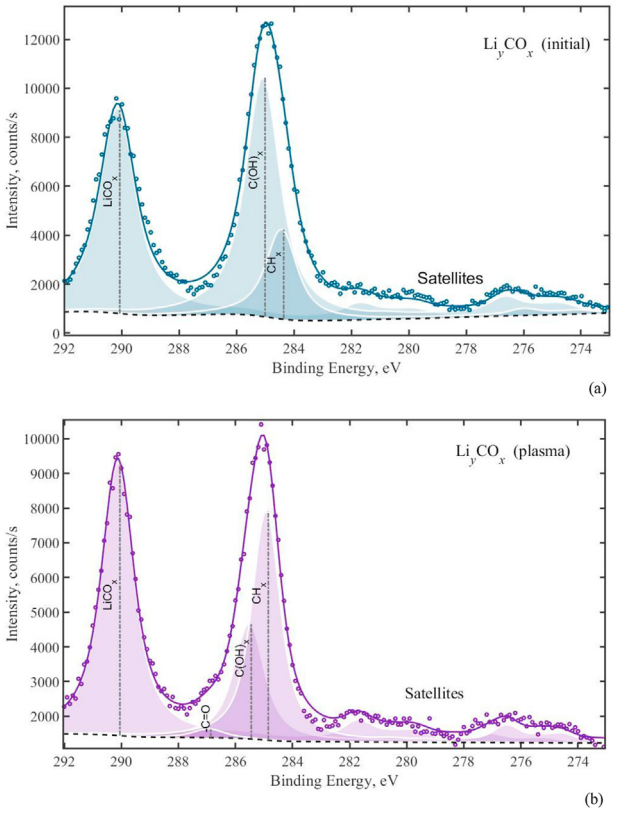

Figure 5. XPS spectra. Line C 1s: (a) initial specimen from the T-10 tokamak, (b) specimen irradiated with plasma in PLM. Filled area - calculated partial peaks; dotted line - background calculated using the method described in [27]; circles -experimental data; solid line – calculated spectrum.

There are only low-intensity peaks in the region of small angles (Figure 7) on the diffraction patterns of the reference industrial powder specimen (Li_{2CO3}). These peaks are characteristics of the hydrogen content in the specimen. Hence, the low intensity indicates a small amount of hydrogen content.

So, hydrocarbons registered by XPS analysis (see above Section) seems to be contained only in a thin surface layer taking into account that the maximum penetration depth of X-ray is of ~5 μm contrary to XPS analysis depth of only a few nanometers.

Diffraction patterns for specimens (T10), (T10-PLM) contain information about lattice constants for Li_2CO_3, which did not change after exposure (there is no peak shift). The plasma irradiation led to sample texturing. The intensity is significantly higher for reflections (130) - $2\theta = 56.280$, (204) - $2\theta = 59.820$, (330) - $2\theta = 67.150$.

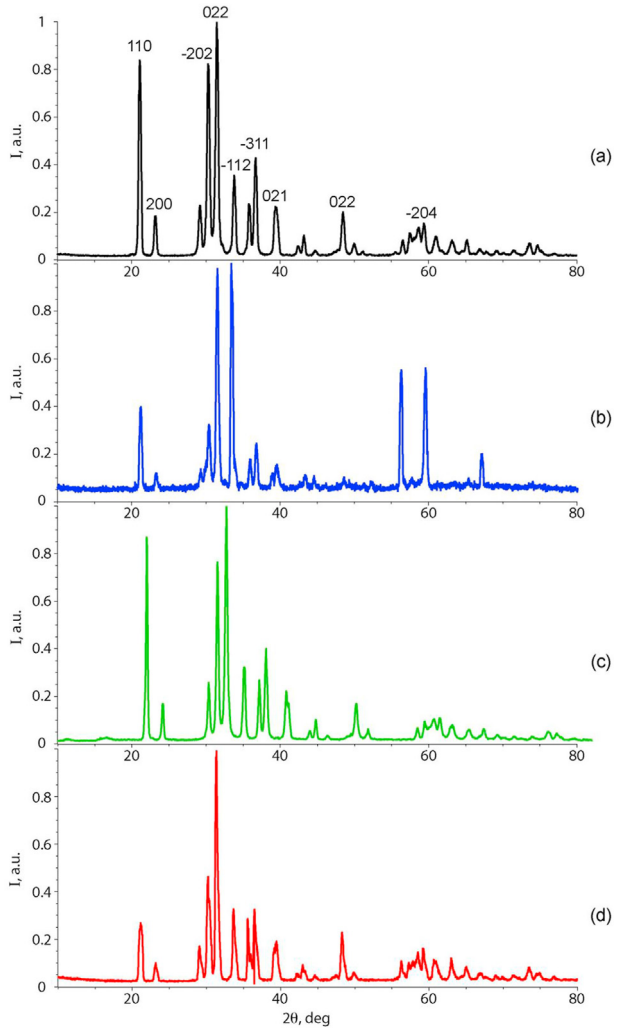

Figure 6. X-ray diffraction patterns of specimens T10 (a), T10 –PLM (b), Li_{2CO3} (c), Li_{2CO3}-PLM (d), the Miller indices (hkℓ) are indicated on the plot.

The crystal structure of specimens from the T10 tokamak is resistant to high-heat plasma irradiation in the PLM device where it was heated up to 700 °C, only the texture was changed under such load.

A comparison of the diffraction patterns of reference industrial Li_2CO_3 specimens before and after plasma exposure in PLM device (Figure 8a) shows that there is a shift of the peaks on X-ray diffraction patterns (Figure 8a), that is the indication of changing the crystal lattice described above.

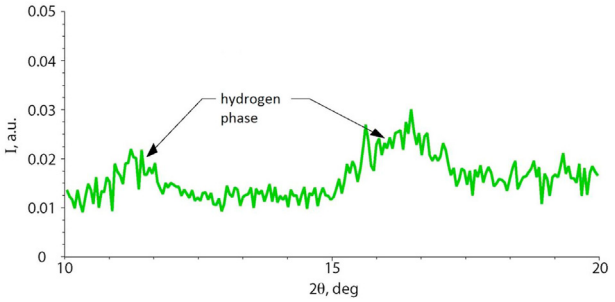

Figure 7. X-ray diffraction pattern of specimen Li_2CO_3.

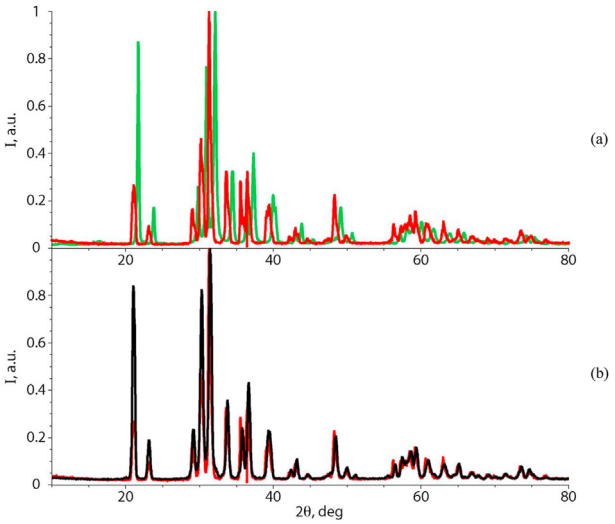

Figure 8. X-ray diffraction patterns of specimens, (a) Li_{2CO3} (green line) and Li_{2CO3}-PLM (red line), (b) Li_{2CO3}-PLM (red line) and T10 (black line).

The crystalline structure of reference industrial Li_2CO_3 irradiated with plasma in PLM device (Li_{2CO3}-PLM) is the same as the structure of specimen (T10) from the T-10 tokamak (Figure 8b).

When comparing the XR diffraction data in Figure 8 we have to pay attention that all peaks for untreated commercial lithium carbonate are shifted relative to the data of all treated samples (see Figure 8a). All samples processed by plasma have the same cell dimensions of the monoclinic lattice which deviates from the structure of reference untreated commercial lithium carbonate Li_{2CO3}. The steady-state plasma irradiation in PLM led to the change of all samples' texturing. The texturing of (T-10) sample match the untreated commercial lithium carbonate Li_{2CO3} (Figure 6c). The subsequent irradiation of (T-10) sample in steady-state plasma of PLM led to the texturing similar to other treated samples (Figure 8b).

The issue of lithium carbonate structure stability under plasma load should be discussed taking into account that solid lithium carbonate is stable up to 1300 °C under ordinary heat load at normal conditions. The specific feature of plasma-facing materials is that there are several processes which simultaneously influence the plasma-surface interaction in devices with high-temperature plasma. The process of plasma-surface interaction in these devices involves numerous mechanisms of intensive surface erosion including melting and resolidification of surface layers, melted material motion and sputtering over surface, sublimation, evaporation, redeposition of the eroded material on the surface, recrystallization, reformation of surface layers from tens of nanometers to hundreds of microns. Even if the surface temperature is less than the melting point, the processes of erosion and evaporation of the material from the surface with subsequent redeposition leads to a surface structure change. In results, a structure of such surface obeys inhomogeneous hierarchical granularity with unusual shape as was recently found in fusion devices [1, 2, 3, 4, 5, 6]. The fact that lithium entered PLM plasma indicates the plasma-induced effect on lithium surface structure rather not only about solid surface remelting or restructuring under high temperature. As well, lithium specimens from the T-10 tokamak were formed under similar conditions when lithium evaporated from the CPS and redeposited together with residual gas on the surface during the long-term process. Such mechanism of lithium deposits growth and effect of the contact with atmospheric gases on the results of XPS and X-ray diffraction data should be investigated in detail in further experiments.

5. Conclusion

Liquid lithium used as the plasma-facing material in the T-10 tokamak evaporated under a powerful plasma load with a duration of ~1 s of plasma discharge and redeposited on the surface resulting in a growth of deposited solid composite films and surface layers with induced self-similar granularity on the scale from macroscales to nanoscale due to strong plasma-surface interaction. Chemical reactions of lithium with impurities in the plasma and on the surface of the vessel led to mixing of materials and a plasma-induced structure. In previous study [21], the post-mortem high-resolution scanning electron microscopy analysis of lithium deposits from the T-10 tokamak and subsequently irradiated with steady-state plasma in PLM device revealed that the surface of all examined samples are strictly irregular with porous and roughen irregular surface, the hierarchical granularity of the structure in the range of scales 0.5–500 μm was observed [20, 21]. The hierarchical structure of deposits within scales from hundreds of nanometers to tens of micrometers of the samples treated in PLM was drastically changed [21].

In present study, X-ray photoemission spectroscopy and X-ray diffraction data analysis of lithium materials irradiated with high-temperature plasma in the T-10 tokamak and the PLM plasma device are used to characterize elemental composition and the difference in cell dimensions of the lattice of treated and untreated materials in comparison with the reference commercial lithium carbonate.

The XPS spectra are used to analyze chemical bonds of elements and the chemical composition of the specimens irradiated with plasma. The X-ray photoemission spectroscopy and X-ray analysis have revealed lithium carbonate Li_xCO_y composites. The stoichiometric formula for lithium carbonate Li_yCO_x is quite different from Li_2CO_3. Such lithium carbonate is able to be formed by absorbing carbon and oxygen from the volume during plasma conditioning or during periods between plasma discharges.

The deposited lithium composites from the T-10 tokamak have been subsequently irradiated with steady-state plasma (~200 min) in PLM plasma device to test the sustainability of lithium deposits under long-term plasma irradiation. Plasma irradiation in PLM device has led to the change of the surface morphology and the elemental chemical composition of specimens from the T-10 tokamak. New structures with a high specific surface area of hierarchical granularity have been registered. The analysis of a reference powder of industrial lithium carbonate irradiated with steady-state plasma in PLM device has demonstrated the universal influence of plasma on the structure of lithium materials.

Other researchers'results (see review [33, 34]) on the matter of lithium carbonate formation in experiments with liquid lithium experiment in tokamaks and steady-state plasma devices are very limited. In Ref. [22] it was found the formation of lithium carbonate on the wall of HT-7 tokamak only after opening the tokamak vessel. In [23] it was proposed that the source of carbon for chemical reactions on the surface might be stainless steel. Li oxidized in experiments with injected lithium granules in EAST tokamak [35].

Mechanism of lithium composite deposits growth and effect of the material's contact with atmospheric gases should be investigated in detail in further experiments.

In a future fusion reactor, the growth of solid lithium chemical composites on in-vessel components can decrease the advantage of liquid lithium components as the first wall.

Declarations

Author contribution statement

V. P. Budaev: Conceived and designed the experiments; Performed the experiments; Wrote the paper.

S. D. Fedorovich: Conceived and designed the experiments; Performed the experiments.

A. V. Lubenchenko: Contributed reagents, materials, analysis tools or data.

A. V. Karpov, N. E. Belova: Analyzed and interpreted the data.

M. K. Gubkin: Performed the experiments.

Funding statement

This work was supported by the Russian Federation Megagrant (14.Z50.31.0042) providing the ASNI on PLM, the Russian Science Foundation (17-19-01469) providing the plasma tests on PLM, the Russian Foundation for Basic Research (19-29-02020) provided the material analysis, ROSATOM (EOTP-223) provided CPS tests, and the Ministry of Science and Higher Education of the Russian Federation (FSWF2020-0023) provided the XPS analysis.

Data availability statement

Data will be made available on request.

Declaration of interests statement

The authors declare no conflict of interest.

Additional information

No additional information is available for this paper.

References

[1] V.P. Budaev, Stochastic clustering of material surface under high-heat plasma load, Phys. Lett. 381 (2017) 3706.
[2] V.P. Budaev, et al., Long-range correlations in the structure of fractal films, JETP Lett. 95 (2) (2012) 78–84.
[3] V.P. Budaev, L.N. Khimchenko, Fractal growth of deposited films in tokamaks, Phys. Stat. Mech. Appl. 382 (2007) 359–377.
[4] V.P. Budaev, Results of high heat flux tests of tungsten divertor targets under plasma heat loads expected in ITER and tokamaks (review), Phys. Atom. Nucl. 79 (7) (2016) 1137–1162.
[5] V.P. Budaev, L.N. Khimchenko, Fractal structure of films deposited in a tokamak, J. Exp. Theor. Phys. 104 (2007) 629.
[6] V.P. Budaev, Stochastic clustering of the surface at the interaction of a plasma with materials, JETP Lett. 5 (10) (2017) 307–312.
[7] A.-L. Barabási, H.E. Stanley, Fractal Concepts in Surface Growth, Cambridge University Press, 1995.
[8] S.V. Mirnov, V.N. Demyanenko, E.V. Muravev, Liquid-metal tokamak divertors, J. Nucl. Mater. 196–198 (1992) 45–49.
[9] A.V. Vertkov, I.E. Lyublinski, Experience in the development of liquid metal plasma facing elements based on capillary-porous structures for a steady-state tokamak (Survey), Phys. Atom. Nucl. 81 (7) (2018) 1000–1007.
[10] V.A. Evtikhin, et al., Lithium divertor concept and results of supporting experiments, Plasma Phys. Contr. Fusion 44 (6) (2002) 955–977.
[11] D. Ruzic, et al., Lithium-metal infused trenches (LiMIT) for heat removal in fusion devices, Nucl. Fusion 52 (2011) 102002.
[12] A.V. Vershkov, et al., Review of recent experiments on the T-10 tokamak with all metal wall, Nucl. Fusion 57 (2017) 102017.
[13] I.E. Lyublinski, et al., Complex of lithium and tungsten limiters for 3 MW of ECR plasma heating in T-10 tokamak. Design, first results, Nucl. Fusion 57 (6) (2017), 066006.
[14] S.V. Mirnov, et al., Li experiments on T-11M and T-10 in support of a steady-state tokamak concept with Li closed loop circulation, Nucl. Fusion 5 (1) (2011) 730449.
[15] G. Mazzitelli, et al., FTU results with a liquid lithium limiter, Fusion Eng. Des. 85 (2010) 896.
[16] G.M. Apruzzese, et al., Spectroscopic measurements for deuterium retention and lithium influx studies with lithium limiter on FTU, Nucl. Mater. Energy 12 (2017) 1214–1218.
[17] H.W. Kugel, et al., NSTX plasma operation with a liquid lithium divertor, Fusion Eng. Des. 87 (2012) 1724.
[18] F.L. Tabarés, et al., Plasma performance and confinement in the TJ-II stellarator with lithium-coated walls, Plasma Phys. Contr. Fusion 50 (2008) 124051.
[19] A.V. Vertkov, et al., Status and prospect of the development of liquid lithium limiters for stellarotor TJ-II, Fusion Eng. Des. 87 (2012) 1755.
[20] V.P. Budaev, et al., Lithium deposits from the T-10 tokamak after experiments with lithium capillary-porous system, J. Phys. Conf. Ser. 1370 (2019), 2nd International Conference on Fusion Energy and Plasma Technologies (ICFEPT2019) 7–9 October 2019, Moscow, Russian Federation.
[21] V.P. Budaev, et al., High-heat flux tests of fusion materials with stationary plasma in the PLM device, Fusion Eng. Des. 155 (2020) 111694.
[22] Zuo, et al., Liquid lithium surface control and its effect on plasma performance in the HT-7 tokamak, Fusion Eng. Des. 89 (2014) 2845.
[23] A. Maan, et al., Plasma facing component characterization and correlation with plasma conditions in lithium tokamak experiment-ß, IEEE Trans. Plasma Sci. 48 (2020) 1463–1467.
[24] V.P. Budaev, et al., Plasma device at NRU «MPEI» for testing of refractory metals and creation of highly porous materials of new generation, VANT ser. Thermoyadernyi sintez 40 (2017) 23.
[25] V.P. Budaev, et al., The plasma device for the high-heat plasma testing of refractory metals and inventing of new highly porous materials, J. Phys. Conf. 891 (2017), 012304.
[26] V.P. Budaev, Investigation of intermittency and generalized self-similarity of turbulent boundary layers in laboratory and magnetospheric plasmas: towards a quantitative definition of plasma transport features, Phys. Usp. 54 (9) (2011) 875–918.
[27] A.V. Lubenchenko, et al., XPS study of multilayer multicomponent films, Appl. Surf. Sci. 427 (Part A) (2018) 711–721.
[28] A.S. Trifonov, et al., Novel electrical transport properties of native Fe-Nb oxide layers leading to unilateral conductivity of a refractory metallic glass, Heliyon 5 (3) (2019), e01424.
[29] A.V. Lubenchenko, et al., Interface layers of Niobium Nitride thin films, J. Phys. Conf. 1410 (2019), 6th International School and Conference "Saint Petersburg OPEN 2019: Optoelectronics, Photonics, Engineering and Nanostructures 22–25 April 2019, Saint Petersburg, Russian Federation.
[30] K. Kanamura, et al., XPS analysis of a lithium surface immersed in propylene carbonate solution containing various salts, J. Electroanal. Chem. 333 (1992) 127–142.
[31] K. Endo, et al., Simulation of C1s spectra of C- and O-containing polymers in XPS by ab initio MO calculations using model oligomers, Polym. J. 29 (1997) 171.
[32] J. Zemann, Die Kristallstruktur von Li2C03, Acta Crystallogr. 10 (1957) 664–666.
[33] R.E. Nygren, F.L. Tabarés, Liquid surfaces for fusion plasma facing components—a critical review. Part I: physics and PSI, Nucl. Mater. Energy 9 (2016) 6–21.
[34] G.S. Zuo, et al., First results of lithium experiments on EAST and HT-7, J. Nucl. Mater. 415 (1) (2011) S1062–S1066.
[35] D.K. Mansfield, et al., First observations of ELM triggering by injected lithium granules in EAST, Nucl. Fusion 53 (11) (2013) 113023.